Organic Electronics 69 (2019) 297–300

Contents lists available at ScienceDirect

Organic Electronics

journal homepage: www.elsevier.com/locate/orgel

Ultrathin, lightweight and flexible organic light-emitting devices with a high light outcoupling efficiency

Xiaheng Huang[a], Yue Qu[a], Dejiu Fan[a], Jongchan Kim[a], Stephen R. Forrest[a,b,c,*]

[a] Department of Electrical Engineering and Computer Science, University of Michigan, Ann Arbor, MI, 48109, USA
[b] Department of Physics, University of Michigan, Ann Arbor, MI, 48109, USA
[c] Department of Materials Science and Engineering, University of Michigan, Ann Arbor, MI, 48109, USA

ABSTRACT

High-efficiency, flexible organic light-emitting diodes (OLEDs) are of interest for display and lighting applications. However, they often suffer from inefficient light extraction, and many outcoupling schemes are incompatible with flexible OLEDs. Here, we demonstrate a corrugated, ultrathin (10 μm), light-weight (20 g/m^2), and flexible OLED on a polychloro-*p*-xylylene (parylene) substrate. A visible-wavelength-scale random corrugation pattern is imprinted on both surfaces of the parylene substrate that efficiently outcouples trapped substrate, waveguide and surface plasmon modes. A green phosphorescent OLED fabricated on a corrugated parylene substrate (CP-OLED) has an external quantum efficiency of 28 ± 2% compared with 21 ± 1% for devices on a conventional flat glass substrate. The CP-OLED shows a Lambertian intensity profile whose spectra are unchanged at different viewing angles. The very thin and flexible substrates offer a solution for foldable displays over very small radii for use in mobile devices and medical applications.

Flexibility is a key advantage of organic electronics. In particular, flexible organic light-emitting diodes (OLEDs) are currently employed in mobile devices, with interest now turning to foldable displays [1–7]. Yet only a few reports on flexible OLEDs [3,5,7] address methods of increasing the light extraction efficiency. Although phosphorescent OLEDs (PHOLEDs) have realized 100% internal quantum efficiency [8,9], the external quantum efficiency (η_{EQE}) of PHOLEDs on flat glass substrates is limited to ~20% due to total internal reflection [10], and losses to absorption, waveguide, and surface plasmon polariton (SPP) modes [11]. To enhance light outcoupling, numerous methods have been advanced, including microlens arrays [12–14] and roughened substrates [15] for extracting substrate modes; sub-anode grids [16] and Bragg diffraction gratings [17] for waveguide modes; and corrugated cathodes or metal-free structures in the active region for surface plasmon polariton (SPP) modes [13,18]. Most of these outcoupling methods, however, have yet to be adapted for use in flexible OLEDs.

Here, we demonstrate ultrathin (10 μm), lightweight (20 g/m^2) and flexible, roughened polychloro-*p*-xylylene (parylene) -based OLEDs with enhanced optical outcoupling. Parylene forms transparent, conformal, pinhole-free and strain-free sheets with good dielectric and mechanical properties [19] that have recently been utilized as flexible substrates for polymer light-emitting diodes (PLEDs) [20], organic photovoltaics (OPVs) [21,22] and OLEDs [23]. In addition, parylene has a relatively high refractive index of $n = 1.64$, which is preferable in terms of outcoupling compared to the commonly used flexible polyethylene terephthalate (PET) substrates [3–7] whose refractive index is $n = 1.57$. A visible-wavelength-scale random corrugation imprinted on both surfaces of the parylene sheet, as shown in Fig. 1a, scatters light from substrate, waveguide and SPP modes. Corrugated parylene OLEDs increase the external quantum efficiency at a current density of $J = 0.1$ mA/cm^2 to $\eta_{EQE} = 28 \pm 2\%$, from $\eta_{EQE} = 21 \pm 1\%$ for analogous OLEDs on flat glass substrates. The thin film OLEDs show a Lambertian intensity profile with identical spectra independent of viewing angle.

The thin film substrate was fabricated by depositing a parylene film on the unpolished side of a sapphire plate. The arithmetic mean roughness of the plate was $R_a = 0.75$ μm, as shown in Fig. 1b, inset. A float-zone glass plate was used to produce a flat parylene substrate for comparison. A solution of 2 vol % Micro-90 detergent in deionized water was spin-coated onto the plates at 500 rpm for 30 s to form a release layer. A double-sided adhesive gel film (PF film X4, Gel-Pak) was cut into an open rectangle and placed onto the plate surfaces. This frame is used as a fixture for peeling off and handling the free-standing parylene films. An 8 μm thick parylene film was deposited via physical vapor deposition (PVD) process at a base pressure of 18 mTorr. Parylene-C dimer (dichloro-[2,2]paracyclophane) was sublimed at 180 °C and cleaved in a pyrolysis furnace at 690 °C into monomeric form. The monomeric gas is then sent into the deposition chamber where it condenses on the plate surfaces to form a conformal coating at room temperature. The parylene film shows birefringence of $\Delta n = -0.04$ (see Fig. S1). A 70 nm thick ITO

* Corresponding author. Department of Electrical Engineering and Computer Science, University of Michigan, Ann Arbor, MI, 48109, USA.
E-mail address: stevefor@umich.edu (S.R. Forrest).

https://doi.org/10.1016/j.orgel.2019.03.040
Received 4 February 2019; Received in revised form 16 March 2019; Accepted 22 March 2019
Available online 23 March 2019

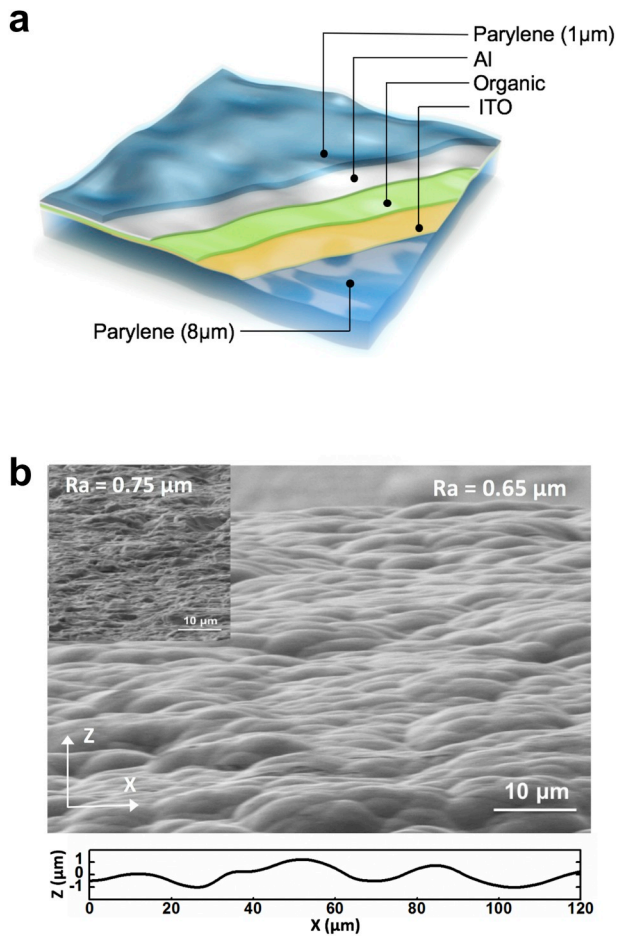

Fig. 1. (a) Illustration of the corrugated parylene-based OLED (CP-OLED). (b) Scanning electron microscope (SEM) image of the corrugated Al cathode surface of the CP-OLED with an arithmetic mean surface roughness of R_a = 0.65 μm. *Inset*, left top: SEM image of the surface of the unpolished sapphire mold with R_a = 0.75 μm; bottom: cross-section of the corrugated cathode measured by confocal laser scanning microscopy.

layer was sputtered onto the parylene surface, followed by thermal evaporation of the organic layers in vacuum at a base pressure of 10^{-7} Torr. The structure of the green bottom-emitting PHOLEDs is: 2 nm MoO_3/40 nm 4,4′-cyclohexylidenebis[N,*N*-bis(4-methylphenyl)benzenamine] (TAPC)/25 nm bis[2-(2-pyridinyl-N)phenyl-C](acetylacetonato)iridium(III) ($Ir(ppy)_2(acac)$) doped at 8 vol % in 4,4′-bis(carbazol-9-yl)biphenyl (CBP)/65 nm 2,2′,2‴-(1,3,5-benzinetriyl)-tris(1-phenyl-1-H-benzimidazole) (TPBi)/1.5 nm 8-quinolinolato lithium (Liq)/100 nm Al. The devices were patterned using a shadow mask comprising an array of 1 mm wide strips, resulting in a crossbar pattern between the bottom ITO and top Al contacts. The devices were encapsulated by depositing a 1 μm thick parylene film over their surfaces. The parylene thickness is calibrated using a profilometer (Dektak XT). The optical constants and thicknesses of other materials were measured using variable-angle spectroscopic ellipsometry. Finally, the flexible OLEDs were peeled off from the plates using the gel frames. Unpeeled samples were also prepared.

The current density-voltage-luminance (*J-V-L*) characteristics of the devices were collected using a semiconductor parameter analyzer (HP-4156A) and a calibrated Si photodiode (Hamamastu, S3584-08). The electroluminescence (EL) spectra were measured using a spectrometer (USB4000, Ocean Optics, Inc). The η_{EQE} was calculated using standard methods [24]. Index-matching fluid (IMF) with an index of refraction of $n_{IMF,\ high}$ = 1.70 was applied between the sapphire substrate (unpeeled sample) and the Si photodiode to detect all air and substrate modes. An IMF with $n_{IMF,low}$ = 1.51 was used for the device on glass.

The optical power distributions within the glass and parylene OLEDs were calculated using Green's function analysis assuming that a dipole emitting at a wavelength of 540 nm is located in the center of the 25 nm thick emissive layer with n = 1.83. $Ir(ppy)_2acac$ dipole alignment leads to 77% normal and 23% horizontal component emission (relative to the substrate plane) [25]. The thicknesses and refractive indices of each layer are: ITO, 70 nm thick, n = 2.1, hole transport layer, 40 nm thick, n = 1.70, electron transport layer, 65 nm thick, n = 1.78, and Al cathode, n = 0.6 + 2.8i. The parylene substrate index is n = 1.64.

A scanning electron microscope (SEM) image of the Al cathode of the CP-OLED is shown in Fig. 1b. The random corrugated pattern originates from the rough surface of the unpolished sapphire substrate that transfers to the conformally deposited parylene film and OLED layers. The transferred corrugation at the CP-OLED cathode has a surface roughness of R_a = 0.65 μm, with a peak-to-valley depth of 2 μm. The relatively spiky features on the unpolished sapphire mold are replaced by a smoothly corrugated profile of the CP-OLED due to the conformal nature of the parylene PVD process.

Fig. 2a shows the *J-V-L* characteristics of the CP/FP (flat parylene)-OLEDs and devices on glass substrates. The CP/FP-OLEDs demonstrate nearly identical *J-V* characteristics compared with both unpeeled and glass substrate devices. The FP-OLED has η_{EQE} = 24 ± 2% at J = 0.1 mA/cm^2, compared to η_{EQE} = 21 ± 1% for the device on the glass substrate. In the CP-OLED, η_{EQE} = 28 ± 2% (see Fig. 2b). The corrugated features of the device have no impact on the electrical properties of the OLED itself since the micron-scale smoothness of the corrugations do not significantly affect the uniformity of the nanometer-scale thicknesses of the OLED active layers.

To understand the source of improvement of the CP-OLED outcoupling from waveguide and SPP modes, we measure all the optical power in the substrate modes using IMF, with results compared in Fig. 2b (triangles). We assume unity transmission at the parylene/sapphire interface. The unpeeled CP-OLED yields η_{EQE} = 49 ± 3%, and the unpeeled FP-OLED yields η_{EQE} = 46 ± 3%. Also, η_{EQE} = 41 ± 3% is obtained for the device on the glass substrate. By subtracting the efficiencies of the glass substrate devices, the enhancement in the extracted waveguide or SPP modes is $\Delta\eta_{CP\text{-}OLED}$ = 8 ± 6% for the CP-OLED, and $\Delta\eta_{FP\text{-}OLED}$ = 5 ± 6% for the FP-OLED.

The electroluminescence (EL) spectra of the devices are shown in the Fig. 2c. All have spectral peaks at $\lambda \approx 530$ nm. The EL spectrum of the FP-OLED shows small oscillations with a period $\Delta\lambda \approx 10$ nm due to interference from the opposite surfaces of the flat, 8 μm thick parylene substrate. This oscillation does not exist for the CP-OLED due to randomization of the optical field by the corrugations. The spectra of parylene-based devices are slightly broader than that using conventional glass substrates due to weaker cavity effects, since the refractive index difference between parylene and the organic layers is small [14]. Photographs of a corrugated (upper) and a flat (lower) parylene substrates on a printed image are shown in Fig. 2c, inset. The flat parylene substrate is transparent while the corrugated one appears hazy due to the random scattering from its roughened surface. Haze can prevent the CP-OLED from use in displays. The angular emission characteristics for the CP-OLED are shown in Fig. 3. Compared to glass-based device, the CP-OLED shows a Lambertian intensity profile. Similarly, the spectral shapes are independent of viewing angle to at least 60° from the substrate normal.

To evaluate the flexibility of the CP-OLED, the performance of the devices was tested before and after bending. The diodes become either leaky or resistive after repeated bending, which is attributed to cracking of the brittle ITO anode [22]. Alternative electrodes are thus required for flexible devices that are capable of bending over sharp angles.

The calculated optical power distributions for the glass and parylene substrate devices are shown in Fig. 4. At an ETL thickness of 65 nm, the high refractive index of the parylene substrate extracts waveguide modes from the organic and anode layers, resulting in more optical

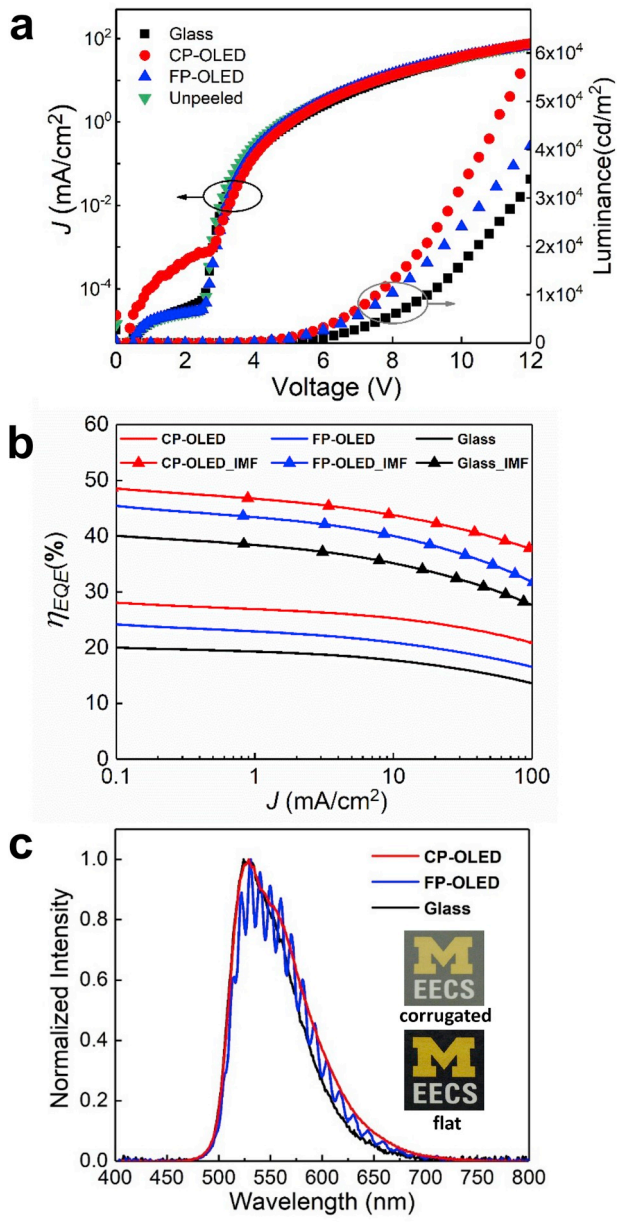

Fig. 2. (a) Current density-voltage-luminance (*J-V-L*) characteristics of the CP/FP-OLEDs, unpeeled and glass devices. (b) External quantum efficiencies (η_{EQE}) of the CP-OLED, FP-OLED, glass and unpeeled devices. The η_{EQE} of the unpeeled CP-OLED, FP-OLED and glass device (triangles) are measured using index-matching fluid (IMF) between the substrate (sapphire for unpeeled CP/FP-OLEDs) and the photodiode to outcouple all substrate modes. (c) Electroluminescence spectra of the devices. *Inset*: Photographs comparing the transparency of the corrugated (upper) and flat (lower) parylene substrates on a printed image.

power trapped inside the substrates compared to glass. By subtracting the calculated power of the substrate modes of the glass from the parylene device, the simulated enhancement in the extracted waveguide modes, $\Delta\eta_{WV\_SIM} = 6\%$, is consistent with our measurements in Fig. 2b, *i.e.*, $\Delta\eta_{FP\text{-}OLED} = 5 \pm 6\%$.

The imprinted corrugated pattern of the CP-OLED randomizes the emitted light trajectories, allowing more of the trapped photons to find the escape cone at all interfaces. The result of this randomization is a Lambertian profile and wavelength-independent emission characteristics. In particular, the corrugated pattern with a visible-wavelength-scale surface roughness of $R_a = 0.65\,\mu m$ effectively enhances the outcoupling of photons within the visible spectrum. Correspondingly, as

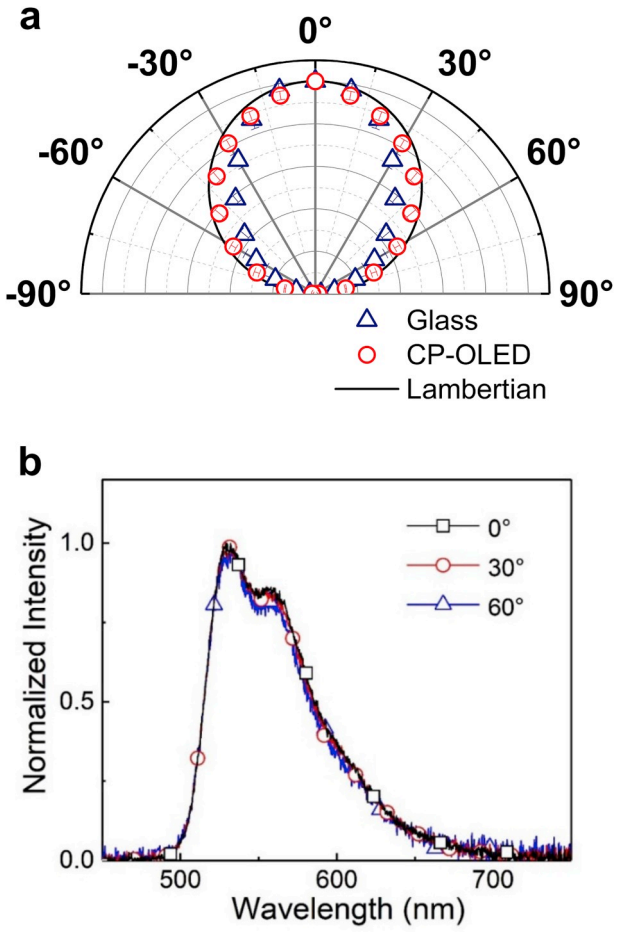

Fig. 3. (a) Angular dependence of light intensity of the CP-OLED and glass-based device. All data are normalized to the intensity in the substrate normal direction. The Lambertian emission pattern is plotted as reference. (b) Electroluminescence spectra of the CP-OLED at viewing-angles of 0°, 30° and 60° to the substrate normal.

shown in the inset of Fig. 1b, the surface profile of the CP-OLED has an approximately 20 μm lateral distance from peak to valley. This structure ensures that the waveguide modes can be effectively scattered out before absorption. The outcoupling efficiencies of CP-OLEDs can be further optimized by using surface molds with optimized roughness, such as sandblasted glass. Compared to other outcoupling schemes implemented in PET-based flexible OLEDs, such as adopting a high-index electrode [3] or introducing gratings/corrugations using nanoimprint lithography [5,7], requiring complicated fabrication processes, our method is simple and has a potentially lower cost.

In summary, we demonstrated ultrathin, lightweight and flexible parylene substrates as a simple and potentially low-cost platform for high-efficiency flexible OLEDs. Outcoupling enhancement is achieved by visible-wavelength-scale corrugations imprinted on the ultrathin high-index parylene substrate. Flexible green PHOLEDs fabricated on corrugated parylene substrates with $\eta_{EQE} = 28 \pm 2\%$ were demonstrated with a Lambertian intensity profile and wavelength-independent emission characteristics. Since the extreme substrate thinness can make handling difficult, in many applications the flexible parylene-based OLEDs can be laminated onto a variety of curved or flat surfaces whose materials choice is unconstrained by device processing conditions. Alternatively, beyond the obvious applications to foldable displays, the thin substrates may serve in medical applications, wearable electronics, or electronic paper where the extreme flexibility is beneficial [21]. Finally, the devices may be compatible with roll-to-roll manufacturing processes, paving the way for widespread and low-cost

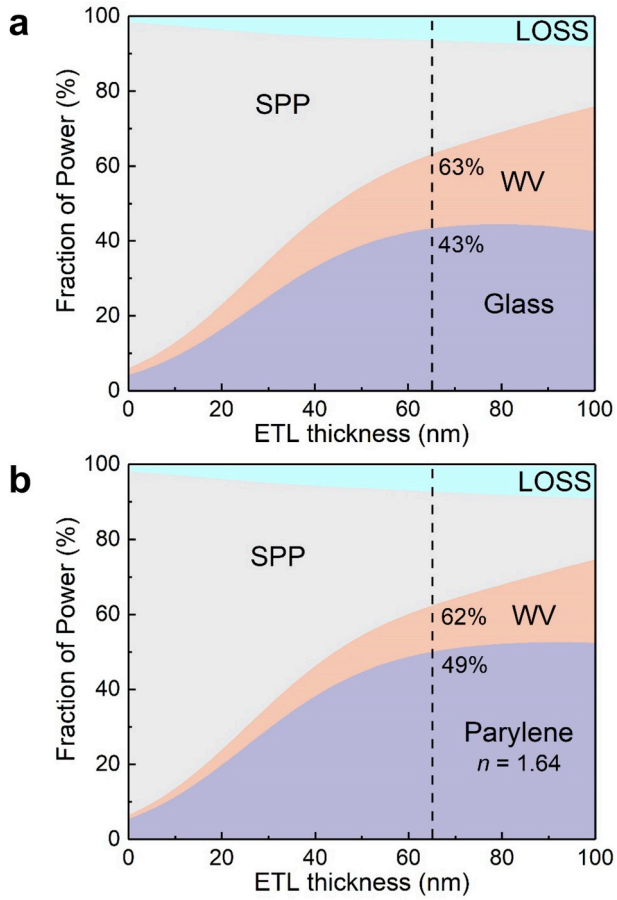

Fig. 4. Optical power modal analysis vs. electron transport layer (ETL) thickness on (a) a conventional glass substrate, and (b) a parylene substrate. The power is distributed into substrate (glass, parylene), waveguide (WV), surface plasmon polariton (SPP) and lossy metal (loss) modes. The ETL thickness used for the devices in this work is 65 nm (dashed line).

use of flexible OLEDs in emerging display and lighting applications.

Acknowledgements

The authors acknowledge the financial support from the US Department of Energy, Solid-State Lighting program under Award DE-EE0007626 and Universal Display Corporation. Part of this work was performed at the Lurie Nanofabrication Facility at the University of Michigan.

Appendix A. Supplementary data

Supplementary data to this article can be found online at https://doi.org/10.1016/j.orgel.2019.03.040.

References

[1] S.R. Forrest, Nature 428 (2004) 911.
[2] G. Gu, P.E. Burrows, S. Venkatesh, S.R. Forrest, M.E. Thompson, Opt. Lett. 22 (1997) 172.
[3] Z.B. Wang, M.G. Helander, J. Qiu, D.P. Puzzo, M.T. Greiner, Z.M. Hudson, S. Wang, Z.W. Liu, Z.H. Lu, Nat. Photon. 5 (2011) 753.
[4] T.-H. Han, Y. Lee, M.-R. Choi, S.-H. Woo, S.-H. Bae, B.H. Hong, J.-H. Ahn, T.-W. Lee, Nat. Photon. 6 (2012) 105.
[5] L.H. Xu, Q.D. Ou, Y.Q. Li, Y.B. Zhang, X.D. Zhao, H.Y. Xiang, J. De Chen, L. Zhou, S.T. Lee, J.X. Tang, ACS Nano 10 (2016) 1625.
[6] L. Zhou, H.-Y. Xiang, S. Shen, Y.-Q. Li, J.-D. Chen, H.-J. Xie, I.A. Goldthorpe, L.-S. Chen, S.-T. Lee, J.-X. Tang, ACS Nano 8 (2014) 12796.
[7] R. Wang, L.H. Xu, Y.Q. Li, L. Zhou, C. Li, Q.D. Ou, J. De Chen, S. Shen, J.X. Tang, Adv. Opt. Mater. 3 (2015) 203.
[8] M.A. Baldo, D.F. O'Brien, Y. You, A. Shoustikov, S. Sibley, M.E. Thompson, S.R. Forrest, Nature 395 (1998) 151.
[9] C. Adachi, M.A. Baldo, M.E. Thompson, S.R. Forrest, J. Appl. Phys. 90 (2001) 5048.
[10] V. Bulovic, V.B. Khalfin, G. Gu, P.E. Burrows, D.Z. Garbuzov, S. Forrest, Phys. Rev. B Condens. Matter 58 (1998) 3730.
[11] P.A. Hobson, S. Wedge, J.A.E. Wasey, I. Sage, W.L. Barnes, Adv. Mater. 14 (2002) 1393.
[12] S. Möller, S.R. Forrest, J. Appl. Phys. 91 (2002) 3324.
[13] Y. Sun, S.R. Forrest, Nat. Photon. 2 (2008) 483.
[14] Y. Qu, J. Kim, C. Coburn, S.R. Forrest, ACS Photonics 5 (2018) 2453.
[15] J. Kim, Y. Qu, C. Coburn, S.R. Forrest, ACS Photonics 5 (2018) 3315.
[16] Y. Qu, M. Slootsky, S.R. Forrest, Nat. Photon. 9 (2015) 758.
[17] W.H. Koo, S.M. Jeong, F. Araoka, K. Ishikawa, S. Nishimura, T. Toyooka, H. Takezoe, Nat. Photon. 4 (2010) 222.
[18] Y. Qu, C. Coburn, D. Fan, S.R. Forrest, ACS Photonics 4 (2017) 363.
[19] M.J. Bak, M. Salcman, E.M.. Schmidt, IEEE Trans. Biomed. Eng. 121 (1977).
[20] T. Yokota, P. Zalar, M. Kaltenbrunner, H. Jinno, N. Matsuhisa, H. Kitanosako, Y. Tachibana, W. Yukita, M. Koizumi, T. Someya, Sci. Adv. 2 (2016) e1501856.
[21] S. Park, S.W. Heo, W. Lee, D. Inoue, Z. Jiang, K. Yu, H. Jinno, D. Hashizume, M. Sekino, T. Yokota, K. Fukuda, K. Tajima, T. Someya, Nature 561 (2018) 516.
[22] J. Jean, A. Wang, V. Bulović, Org. Electron. Phys. Mater. Appl. 31 (2016) 120.
[23] J.-H. Lee, A. Kim, Org. Electron. 47 (2017) 147.
[24] S.R. Forrest, D.D.C. Bradley, M.E. Thompson, Adv. Mater. 15 (2003) 1043.
[25] M.J. Jurow, C. Mayr, T.D. Schmidt, T. Lampe, P.I. Djurovich, W. Brütting, M.E. Thompson, Nat. Mater. 15 (2016) 85.